# An Efficient, Robust New Scheme for Establishing Broadband Homonuclear Correlations in Biomolecular Solid State NMR

# An efficient, robust new scheme for establishing broadband homonuclear correlations in biomolecular solid state NMR

Dr. Sungsool Wi[1]* and Prof. Dr. Lucio Frydman[1,2]

[1] National High Magnetic Field Laboratory, Tallahassee, Florida 32304, USA

[2] Department of Chemical and Biological Physics, Weizmann Institute of Sciences, Rehovot, Israel

**Abstract**

An efficient mixing scheme is here introduced for establishing two-dimensional (2D) homonuclear correlations based on dipolar couplings, that achieves broadband dipolar recoupling using remarkably low powers even under ultrafast magic-angle spinning (MAS) rates. This Adiabatic Linearly FREquency Swept reCOupling (AL FRESCO) method applies a series of weak frequency-chirped pluses on the $^{1}$H channel, for performing efficient $^{13}$C-$^{13}$C magnetization transfers leading to cross peaks between sites separated over small or large chemical shift differences. This mixing scheme is nearly free from dipolar truncation effects, and thanks to the low RF powers it involves it can act over long mixing times (≥1.5 sec). Key considerations required for optimizing this chirped pulse mixing scheme are discussed, and the new kind of correlations that can emerge from this method are demonstrated using uniformly $^{13}$C-labeled Barstar as test protein sample.

**Keywords:** Spectroscopic Methods, NMR spectroscopy, biophysics, solid state structures

## 1. Introduction

Continuous technological and conceptual developments have endowed contemporary high-resolution solid-state nuclear magnetic resonance (NMR) spectroscopy, with capabilities that rival those of solution-state NMR when tackling structural and dynamic investigations of large biomolecules [1-8]. When performing such studies the problem of spectral assignment and resolution nearly invariably arises, demanding the use of high-dimensional NMR experiments correlating labeled $^{13}$C- and/or $^{15}$N sites in the biomolecule. This in turn often calls for reintroducing the dipolar interactions among these labeled nuclei, that are otherwise averaged out by the magic-angle-spinning (MAS) procedure that is required for achieving site-specific high-resolution information in this kind of study. The reintroduction of these dipolar interactions can be spontaneous as in Rotational Resonance [9] or Proton-Driven Spin Diffusion (PDSD) [10-12], or requires an RF pulse scheme that interferes with the MAS modulation [13-16]. The latter can in turn center on the targets of observation ($^{13}$C, $^{15}$N) [15,17-19], or, as the majority of $^{13}$C-$^{13}$C recoupling methods thus developed, center at reintroducing these homonuclear interactions by manipulating the $^{1}$Hs that are widely present in this kind of system. Of particular significance among these methods are those that recouple homonuclear interactions without being subjected to dipolar truncation effects [20]—a phenomenon whereby strong interactions resulting from a (usually directly bonded) dipolar coupled pair, eliminate the weak but structurally crucial information coming from long-range ($r_{CC} \geq 3$Å) dipolar couplings. Homonuclear recoupling methods thus developed that are tolerant to dipolar truncation effects include Stochastic Dipolar Recoupling (SDR) [21], Dipolar Assisted Rotational Resonance (DARR) [22,23], RF-assisted Diffusion (RAD) [24], and Proton Assisted Recoupling (PAR) [25,26]. PDSD, DARR and RAD have been widely used as core methods in structural biology, as the setting of these experiments is straightforward and the signal transfers between sites of interest can be obtained robustly and for long mixing times [27-32]. These methods, however, begin to fail as MAS rates exceed ≥30 kHz; i.e., as the MAS rates become significantly larger than the chemical shift differences between $^{13}$C pairs [23,33]. This has led to the advent of recoupling methods capable of operating at higher MAS rates, including DARR variants such as Phase-Alternated Recoupling Irradiation Scheme (PARIS) [34], PARIS$_{xy}$ [33], Second-order Hamiltonian among Analogous Nuclei Generated by Hetero-nuclear Assistance Irradiation (SHANGHAI) [35], Second-order Hamiltonian among Analoguous nuclei Plus (SHA+) [36-38], and COmbined $R2_n^{\nu}$-Driven (CORD) [39,40]. Best

performing among these are usually the latter methods, such as SHA+ and CORD, which can deliver $^{13}C$-$^{13}C$ cross-peaks at MAS rates $\nu_r \geq 40$ kHz while covering a wide chemical shift frequency range. As MAS rates increase further, however, the rf pulse strengths of these mixing schemes (which increase in proportion to $\nu_r$) become significant, thereby placing a limit to the mixing time durations that can be employed in these experiments before RF sample heating sets in. Although transverse magnetizations have to be used for mixing, the PAR method also has been successfully employed at high speed MAS spinning rates.

This manuscript introduces a new scheme, Adiabatic Linearly FREquency Swept reCOupling (AL FRESCO), that produces $^{13}C$-$^{13}C$ dipolar correlations between sites spanning a very large range of chemical shift offsets, is nearly insensitive to dipolar truncation effects, and operates under very weak RF field strengths. The AL FRESCO mixing scheme operates at any MAS rate, but is particularly advantageous at the ultrafast rates and long mixing time conditions that challenge most other schemes. As many of the previously mentioned methods, AL FRESCO also relies on a second-order recoupling mechanism, whereby $^{1}H$-$^{13}C_1$ dipolar recoupling assists the reintroduction of $^{13}C_1$-$^{13}C_2$ rotational resonance effects. In certain aspects it resembles most the Mixed Rotational and Rotary Resonance (MIRROR) [41] scheme, where an amplitude-modulated adiabatic rf pulse is applied along the proton channel to extend the range of $^{13}C$ recoupling conditions over a range of offset frequencies. The AL FRESCO mixing scheme, however, applies a frequency-swept (chirped) rather than an amplitude-modulated pulse on the proton channel, during the mixing period $\tau_{mix}$. This leads to a variety of parameters defining the pulse shape (amplitude, sweep bandwidth, duration, sampling dwell time) whose settings aid greatly in optimizing the transfers and resulting correlations.

## 2. Experimental

**2.1 Sample:** Barstar was produced and purified as described by Schreiber *et al* [42]. In brief, a culture of BL21(DE3)pLysS harboring a plasmid encoding a mutated barstar (C40A, C82A) was grown in M9 minimal medium supplemented with 1 g/L $^{15}N$-labeled ammonium chloride, Ampicillin (100 μg/mL) and Chloramphenicol (17 μg/mL). The culture was induced at $OD_{600}$ 0.6 with 200 μM isopropyl β-D-1-thiogalactopyranoside (IPTG) and grown overnight at 30 °C. Barstar was isolated by precipitation with 40-80% ammonium sulfate, injected to a gel filtration column (Hiload_Superdex_75_26/60, GE Healthcare), and pre-equilibrated with the same buffer.

Final purification on an anion exchange column (HiTrap_Q_HP, GE Healthcare) involved elution with 300 mM NaCl. The fractions containing Barstar were dialyzed to deionized water and lyophilized. For the NMR experiments, about 2.8 mg and 11 mg of the protein sample were packed into Bruker 1.3 mm or Bruker 2.5 mm MAS rotors, respectively, for the experiments.

**NMR experiments:** Experiments were carried out on 14.1 T and 11.7 T magnets equipped with Bruker Neo and AvanceIII consoles, respectively. Temperatures were stabilized at ≈10 ºC by flowing a nitrogen gas stream through an FTS cooling system. A 1.3 mm probe was used at 14.1 T for performing MAS at $\nu_r = 60$ kHz, and a 2.5 mm probe was used at 11.7 T for spinning at $\nu_r =$ 12 kHz; the former showed a minor impurity signal in the 70-80 ppm region of unknown origin. Figure 1 shows the AL FRESCO mixing scheme that was implemented, as incorporated within the framework of a standard two-dimensional (2D) homonuclear $^{13}$C dipolar correlation spectroscopy. The frequency chirps employed in the AL FRESCO mixing schemes were based on WURST-shaped pulses [43,44], with their quadratic phase modulation defined by a frequency sweep bandwidth BW. These were clocked out with a sampling dwell time $\Delta t$ for an overall duration $t_p$, chosen as described in Theoretical Considerations. In some of the tests the AL FRESCO mixing time $\tau_{mix}$ involved multiple chirped pulses; for those cases $\tau_{mix} = nt_p$ ($n$ = 2, ...); the sense of the sweeps was repeatedly alternated; and an XY-$n$ phase alternation scheme was used [45]. The $^1$H and $^{13}$C 90º pulses were 2.5 and 5 μs, respectively, for all experiments. Optimal CP conditions were found at $\nu_{1C} = 41$ kHz with $\nu_{1H} = 12$ kHz when $\nu_r = 60$ kHz and at $\nu_{1C} = 42$ kHz with $\nu_{1H} = 84$ kHz when $\nu_r = 12$ kHz; a ramped (70%-110%) spin-lock pulse along the $^1$H channel was used for CP [46,47], while simultaneously applying a rectangular pulse on the $^{13}$C. The optimized CP time for all cases was 1 ms. The $^1$H decoupling scheme applied during the direct and indirect acquisition periods was $XiX_{45}$ [48,49] ($\nu_{1H}$ = 16 kHz) at $\nu_r$ = 60 kHz, and SPINAL-64 [50] ($\nu_{1H}$ = 90 kHz) at $\nu_r$ = 12 kHz. 2D $^{13}$C-$^{13}$C correlation spectra were also measured by CORD at $\nu_r$ = 60 kHz (14.1 T) as well as by DARR at $\nu_r$ = 12 kHz (11.7 T). The $^1$H RF field strengths used in the CORD mixing period for the $R2_1^1R2_1^2$ blocks and the $R2_2^1R2_2^2$ blocks were 60 kHz and 30 kHz, respectively. The $^1$H RF field strength used in the DARR mixing period [22,23] was 12 kHz.

**Numerical simulations:** All simulations were carried out by considering the MAS-modulated internal Hamiltonians and the external RF Hamiltonian in the rotating frame. All isotropic and anisotropic chemical shifts as well as the homonuclear and heteronuclear dipolar interactions

involved in the spin system under consideration were considered as their usual Hamiltonians, without any truncation approximation. Powder averaging of all anisotropic interactions were carried out by considering the 6044, 3722, or 1154 orientations of the ZCW's Euler angle sets [51], and assuming coincident dipolar and CSA tensors for simplicity. The performance of the AL FRESCO mixing scheme was calculated numerically by considering the time propagation of the density matrix in terms of a piecewise time increment. The $\Delta t$ dwell time of the chirp pulse digitization was also explicitly considered as part of these simulations.

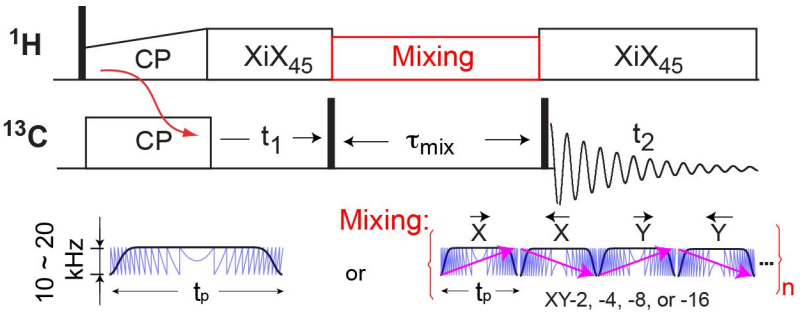


**Figure 1.** AL FRESCO mixing scheme incorporated within the standard platform of 2D $^{13}$C homonuclear correlation spectroscopy. AL FRESCO employs a phase-modulated linear frequency chirped pulse or a train of chirped pulses applied on the $^{1}$Hs, with optimal RF pulse strengths of ≈10~20 kHz regardless of the MAS rate used. When using a train of chirped pulses, the mixing scheme benefits from concatenating forward- and backward-sweeps while employing an XY-*n* phase-alternation scheme [45] to compensate potential RF inhomogeneities.

## 3. Theoretical Considerations

**3.1 The AL FRESCO recoupling: Bandwidth and dwell-time chirp considerations.** Figure 2 shows 3D mesh plots of the offset-frequency dependent $C_1 \rightarrow C_2$ signal transfer profiles for the AL FRESCO mixing scheme introduced in Figure 1. These polarization transfer characteristics were calculated by brute-force numerical simulations that assumed an $H_1$-$C_1$-$C_2$-$H_2$ spin system, employing different $\Delta t$ and BW values under $\nu_r = 60$ kHz of MAS spinning rate. The plots show intensity build-ups of the $C_{2z}$ polarization being received (z-axis) as a function of a mixing time $\tau_{mix}$ ranging from 0 to $t_p$ (a single chirped pulse was assumed for the mixing), upon varying the offset-frequency difference $\Delta\Omega = \Omega_{C2} - \Omega_{C1} (\Omega_{C1} = 0)$ between the two $^{13}$Cs. Notice the strong dependence of AL FRESCO's $^{13}$C polarization transfer dynamics on the dwell used to clock out the $^{1}$H chirped pulse, evidencing harmonics with a more efficient $^{13}C_1 \rightarrow {}^{13}C_2$ transfer for a variety of $\Delta\Omega$ $^{13}$C offsets depending on the $\Delta t$ value used. When using small $\Delta t$ values (e.g., 5 μs) that faithfully represent the frequency sweep, a relatively small number of harmonic modes are generated. By contrast, for bigger $\Delta t$ values (e.g., Δt = 60 μs) that may break

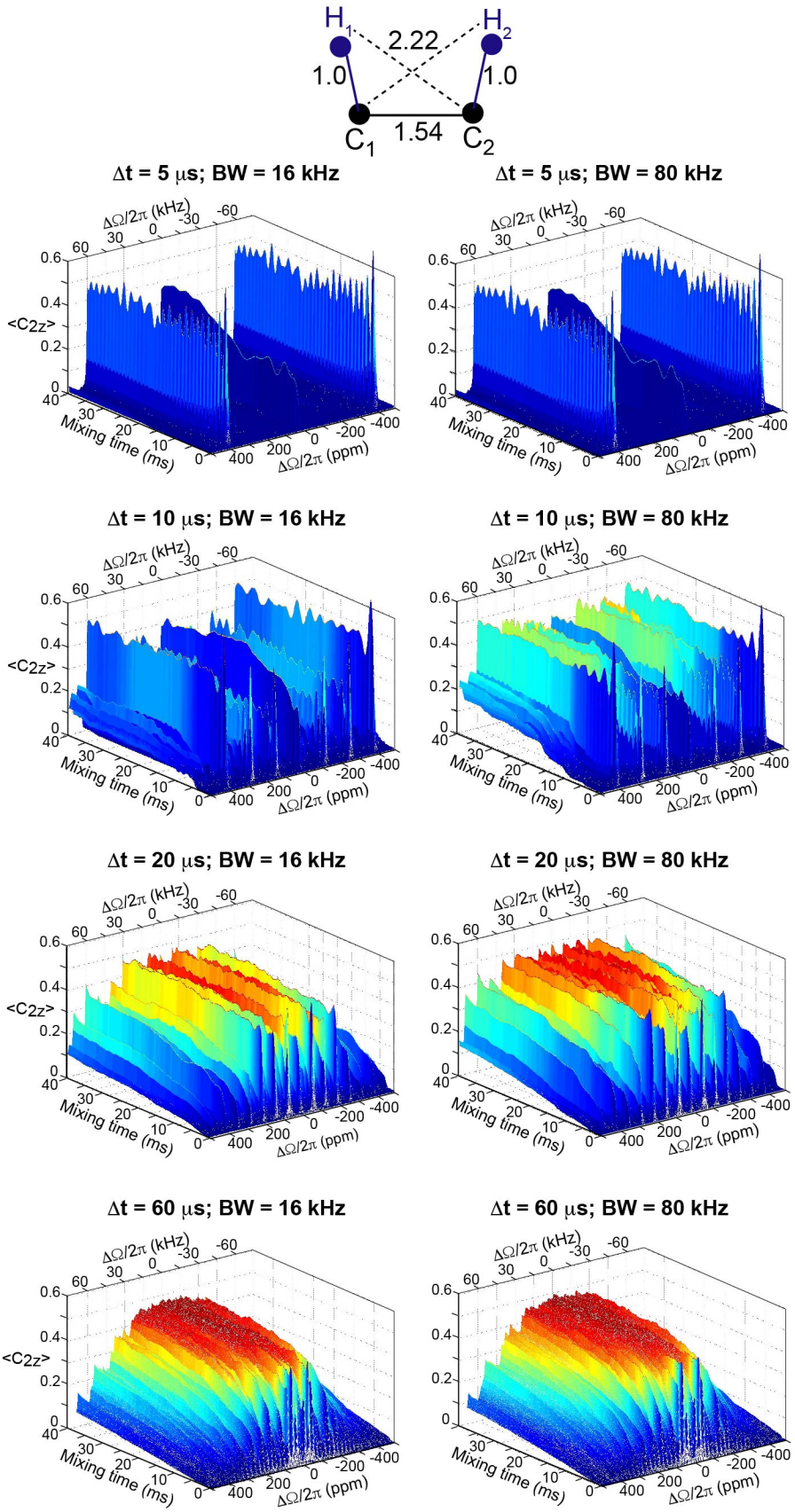


**Figure 2.** Development of the $C_{1z} \rightarrow C_{2z}$ polarization transfer dynamics arising from an initial state $C_{1z}=1$, $C_{2z}=0$, when monitoring $C_{2z}$ as a function of mixing time $0 \leq \tau_{mix} \leq t_p = 40$ms, for a range of offset frequencies $-500\text{ppm} \leq \Omega_{C2} \leq 500\text{ppm}$ while assuming $\Omega_{C1} = 0$. The plots were calculated as a function of the chirp pulse bandwidth (BW) and its sampling dwell ($\Delta t$), for an AL FRESCO mixing scheme like the one in Figure 1. Additional assumptions involved a four-spin system $H_1$-$C_1$-$C_2$-$H_2$ (top, numbers indicating distances in Å) undergoing MAS at $\nu_r = 60$ kHz. Additional parameters included $\delta_{CSA}^{C1} = \delta_{CSA}^{C2} = 40$ ppm, $\eta_{C1} = \eta_{c2} = 0.3$, $\delta_{ISO}^{H1} = -2$ ppm, $\delta_{CSA}^{H1} = 3$ ppm, $\eta_{H1} = 0$, $\delta_{ISO}^{H2} = 4$ ppm, $\delta_{CSA}^{H2} = 2$ ppm, $\eta_{H2} = 0.2$, $\nu_0[^1\text{H}] = 600$ MHz; $\nu_0[^{13}\text{C}] = 150$ MHz, $\nu_{1H} = 15$ kHz. Exact distances were $r[C_1\text{-}C_2] = 1.54$ Å, $r[C_1\text{-}H_1] = 1.00$ Å, $r[C_2\text{-}H_1] = 2.22$ Å, $r[C_1\text{-}H_2] = 2.22$ Å, $r[C_2\text{-}H_2] = 1.00$ Å, $r[H_1\text{-}H_2] = 2.54$ Å. Notice the strong harmonic recoupling modes formed in the offset-frequency profile, as well as their Δt-dependence.

the Nyquist demands for a faithful frequency sweep, a large number of contiguous harmonic modes are generated. This in turn widens the range of offsets that provide a robust $C_1 \rightarrow C_2$ polarization transfer making the latter independent of the $^{13}C$'s precise frequency positions; broad-bandness vis-à-vis the $^{1}H$ chemical shift is endowed by the reliance of $^{1}H$ frequency chirped pulses. This is a rather unusual feature arising in this sequence: RF frequency sweeps are usually programmed as quadratic phase tables, sampled at $\Delta t$ increments such that $1/\Delta t >$ BW. However, as shown by the simulations in Figure 2 and further expanded by the buildups in Figure 3, the efficiency of the AL FRESCO mixing can be increased if subsampled BW > $1/\Delta$t conditions are employed for clocking out the chirped pulses. We ascribe this to a repeated foldover action whereby the phenomena defining the $C_1 \rightarrow C_2$ polarization transfer, arise numerous times over the course of the undersampled swept pulse. As each of these times the recoupling will act with limited efficiency, repeating them with the pseudo-random phases provided by an undersampled chirp, ensures a more effective recoupling whose overall effect is somewhat akin to a stochastic-like action [21]. Supporting Information Figure S1 presents additional substantiations of this issue).

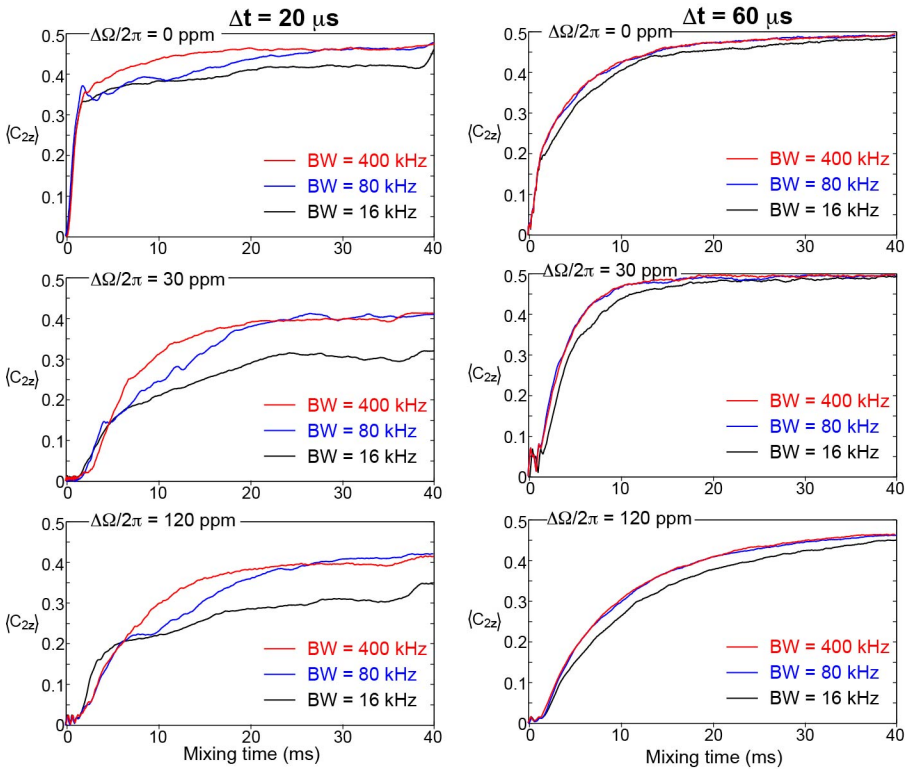


**Figure 3.** The influence of BW and $\Delta t$ on AL FRESCO's $C_1 \rightarrow C_2$ polarization transfer dynamics calculated on a $H_1$-$C_1$-$C_2$-$H_2$ spin system (Fig. 2) under $\nu_r$ = 60 kHz. For both cases the $C_{2z}$ buildup is calculated as a function of mixing time $\tau_{mix}$, $0 \leq \tau_{mix} \leq t_p$=40 ms ($C_{1z}$ = 1 and $C_{2z}$ = 0 at $\tau_{mix}$ = 0) at three different offset frequencies ($\Delta\Omega/2\pi$ = 0, 30, and 120 ppm; $\nu_0(^{13}C)$ = 150 MHz). Notice that sampling the pulse at a rate that satisfies the Nyquist criterion for all BWs yields a in general a slower $C_{1z} \rightarrow C_{2z}$ polarization transfer efficiency than upon breaking this criterion –which in turn results in multiple foldovers within the frequency window $1/\Delta$t.

Inspection of the frequency gaps between adjacent harmonic modes (Fig. 2 and Supporting Information 1) suggests that these will be spaced (in ppm) by small, non-zero values of

$$\Delta\Omega = |g\nu_r - l/\Delta t|/\nu_0. \quad (1)$$

For instance, when considering the $\Delta t$ = 10 μs, $\nu_r$ = 60 kHz, $\nu_0[^{13}C]$ = 150 MHz case in Fig. 2, Eq. (1) predicts this gap for $g$ = 1 and $l$ = 2, according to $|1 \times \nu_r - 2/\Delta t|$ /$\nu_0$ = 133 ppm. As detailed in the Supporting Information, frequency gaps predicted for the other cases in Fig. 2 are 400 ppm ($g$=9,$l$=3), 66.7 ppm ($g$=1,$l$=1), and 22.2 ppm ($g$=7,$l$=2) for $\Delta t$ = 5 μs, 20 μs and 60 μs, respectively. These gaps agree with the data shown in Figure 2. The simulations in Fig. 2 also suggest that the BW value used in the chirps has a smaller influence in these harmonics' positions, but rather determines how quickly the $C_1$-$C_2$ transfer occurs for a given $\nu_r$ and $\Delta t$.

**3.2 DARR- and MIRROR-like effects arising with chirped pulses.** While a more complete analysis of these polarization transfer phenomena will be given in an upcoming publication, it is worth to briefly dwell on the physics underlying them. For simplicity we consider a case where a single chirp pulse is applied along the $^1$H channel, to interfere with the averaging that otherwise MAS will perform on the $^{13}$C-$^{13}$C dipolar couplings. This sweep will also involve weak rf fields ($\nu_{1H}$≈10-20 kHz) –much smaller than the $\nu_{lH} \approx \nu_r$ that would have to be met to achieve the DARR-like $^1$H-$^{13}$C recoupling that normally facilitate $^{13}C_1 \Leftrightarrow {}^{13}C_2$ polarization exchanges. On the other hand it is sufficient for the effective $^1$H nutation field $\nu_{eH}(t) = \sqrt{\nu_{1H}^2 + [\Delta\nu_H(t)]^2}$ to match $\nu_r$ in order to reintroduce at least in part the DARR conditions; as the $^1$H off-resonance field is swept as a function of time as $\Delta\nu_H(t) = \frac{\mathrm{BW}}{2} - \left(\frac{\mathrm{BW}}{t_p}\right)t$, the condition $\nu_{eH}(t) = \nu_r$ is surely met at two (or if undersampling the chirp, at multiple) points during the mixing process. Assuming for simplicity a three-spin system $^1$H-$^{13}C_1$-$^{13}C_2$ with $^1$H-$^{13}C_1$ and $^{13}C_1$-$^{13}C_2$ but no $^1$H-$^{13}C_2$ dipolar couplings, the ensuing rotary resonance imposed along the $^1$H will broaden the $^{13}C_1$-$^{13}C_2$ rotational resonance effect on its coupled $^{13}C_1$ as [22,23]

$$\Xi(t) = \frac{2}{T_r}\frac{b_{C_1,H}(t)\nu_{1H}}{[\nu_{eH}(t)]^2}, \quad (2)$$

where $T_r$ is the MAS rotor period and $b_{C_1,H}(t)$ is the orientation-dependent, MAS-modulated H-$C_1$ dipolar coupling. This broadening will in turn facilitate the homonuclear zero-quantum (flip-flop) transfer process between $C_1$ and $C_2$ for crystallites fulfilling the condition [22,23]

$$\Delta\Omega = |k\nu_r - \Xi(t)|, \tag{3}$$

where $\Delta\Omega = \Omega_{C2} - \Omega_{C1}$ is the offset-frequency difference between the $^{13}$Cs and $k$ = 1 or 2. The chirp time at which this acceleration of the $C_1$-$C_2$ polarization transfer occurs does not need to be identical with that facilitating the classical DARR effect (given by the $\Xi(t) = \frac{1}{T_r}\frac{b_{C_1,H}(t)}{\nu_{1H}}$ condition); as discussed by Takegoshi, Ernst and others [23,39,41], Eq. (3) further broadens the range of $^{13}$C offset differences $\Delta\Omega$ at which this process will happen. The AL FRESCO experiment, however, brings another time-dependency that assists in broad-banding its efficiency, and it is the dwell time $\Delta$t with which the RF is swept. In general, these dwells $\Delta t$ ($= t_p/N$, where $t_p$ is the chirp pulse's duration and $N$ its number of sampling points) are chosen much smaller than the inverse bandwidth of the sweep, so as to achieve a faithful reproduction of the instantaneous frequencies. As detailed in Figs. 2 and 3 (and as observed in experiments, *vide infra*) the $\Delta t$-dependence provides AL FRESCO with an additional way of interfering with the MAS averaging of the homonuclear magnetization transfer. This interference endows an additional $\Delta$t-dependency onto the $\Xi(t)$ broadening, breaking it into sidebands. As the magnitude of $\nu_{eH}(t)$ varies throughout the course of the sweep, the interference effect provided by Eq. (3) will then be present for a wider range of $^{13}$C chemical shift differences meeting a revised rotational resonance condition:

$$\Delta\Omega(t) = \pm j\left|k\nu_r - \frac{l}{\Delta t}\frac{2b_{C_1,H}(t)\nu_{1H}}{[\nu_{eH}(t)]^2}\right|, \tag{4}$$

where $j$ = 0, 1, 2…, $\Delta$t = $l\times T_r$, and $k$ and $l$ are positive integers.

In addition to this first-order effect, $^1$H-mediated recoupling between the $^{13}$Cs is also aided by a 2$^{nd}$-order interference between the time-dependent homonuclear $^{13}C_1$-$^{13}C_2$ and the heteronuclear $^1$H-$^{13}C_1$ dipolar interactions –the so-called MIRROR effect [41]. In this case interference will arise between the periodic modulations that MAS will impose on the aforementioned homo- and hetero-nuclear interactions, and the additional time modulation that, at a rate $\nu_{eH}(t)$, the applied

chirped RF pulses will impose on the $^{1}H$-$^{13}C_1$ coupling. As a result of all these effects, an additional time-dependent condition

$$\Delta\Omega(t) = \pm j[m\nu_r - \nu_{eH}(t)]; \quad m = \cdots -2, -1, 1, 2 \ldots \tag{5}$$

will also arise over a wide offset frequency range, where the exchange of magnetization between the coupled $^{13}Cs$ is facilitated.

**3.3 Optimizing AL FRESCO's chirped pulse.** If combining the above-mentioned rotational resonance and MIRROR effects, it follows that the $C_1$-$C_2$ polarization transfer harmonics will occur at various time-dependent offsets satisfying

$$\Delta\Omega = \pm j \left| (m+k)\nu_r - \frac{l}{\Delta t}\frac{2\langle b_{C_1,H}(t)\rangle \nu_{1H}}{[\langle \nu_{eH}(t)\rangle]^2} - \langle \nu_{eH}(t)\rangle \right|. \tag{6}$$

When considered over the duration of the mixing time and over a powdered sample, the frequency profile of the $\Delta\Omega$ recoupling profile will thus be dominated by sidebands at $|g\nu_r - l/\Delta t|$, where $g = m + k$. For these offsets polarization exchanges among crystallites whose orientations satisfy $2\langle b_{C_1,H}(t)\rangle \nu_{1H} = [\langle \nu_{eH}(t)\rangle]^2$ will be facilitated, where $\langle b_{C_1,H}(t)\rangle$ and $\langle \nu_{eH}(t)\rangle$designate time- and powder-averaged H-$C_1$ dipolar couplings and effective $^{1}H$ nutation fields, respectively. In order to minimize the frequency gaps between these harmonic polarization transfer modes it is convenient to adjust the $\Delta t$ value employed to sample the chirped RF sweep for a chosen MAS spinning rate $\nu_r$, so that $|g\nu_r - l/\Delta t|$ is minimized. This results in a uniform, broad-banded offset-frequency recoupling profile for the $C_1 \rightarrow C_2$ polarization transfer.[1] The predictions of Eq. (6) qualitatively match the trends evidenced by the numerical simulations in Fig. 2 which show that for a given $\nu_r$, there exists an optimal $\Delta t$ and a certain combination of $g$ and $l$ integer values that minimize the $|g\nu_r - l/\Delta t|$ term; this condition will in turn maximize the number of harmonics fitting within a given frequency window, and enhance the recoupling's robustness. Moreover, as each of these harmonics has a certain time- and powder-averaged width $\langle \Xi \rangle$, this kind of interference between the MAS and the chirped pulse modulations provides AL FRESCO with a highly homogeneous offset coverage for the $^{13}C$-$^{13}C$ polarization transfers.

[1] The linear $\nu_{eH}(t)$ term in Eq. (6) provides an additional transfer mode on top of the aforementioned adjacent harmonic modes, as described in the next paragraph.

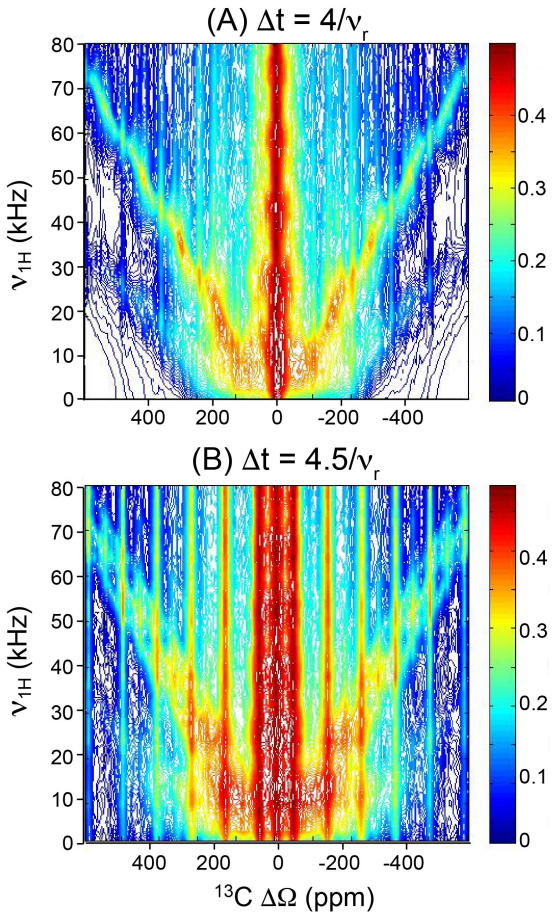


**Figure 4.** RF field ($\nu_{1H}$) dependence for AL FRESCO recoupling (y-axis) as a function of the $\Delta\Omega = \nu_{iso}^{C1} - \nu_{iso}^{C2}$ separation between the $^{13}C$ (x-axis). The plots calculate the $C_{1z}\rightarrow C_{2z}$ transfer efficiency for a $H_1$-$C_1$-$C_2$-$H_2$ spin system (as in Fig. 2; colormap indicates $<C_{2z}>$), assuming a single chirp recoupling with BW = 80 kHz, $t_p$ = 40 ms, and two different sampling conditions: $\Delta t$ = 66.67 μs ($4/\nu_r$, A), and $\Delta t$ = 75 μs ($4.5/\nu_r$, B).

**3.4 RF field strength considerations:** AL FRESCO is not based on 90° pulses or on adiabatic inversions; in fact, it was experimentally found that $\nu_{1H}$≈5∼20 kHz leads to the most efficient recoupling –nearly regardless of the MAS rates used. Further insight into this unusual dependence can be gathered from the numerical simulations shown in Fig. 4, which describe how the $C_{1z}\rightarrow C_{2z}$ polarization transfer efficiency changes with RF field strength $\nu_{1H}$ and with the resonance frequency difference ΔΩ between $C_1$ and $C_2$, for $\Delta t$ values of 66.67 μs ($4/\nu_r$, A) and 75 μs ($4.5/\nu_r$, B) and for otherwise identical BW (80 kHz), $t_p$ (40 ms) and $\nu_r$ (60 kHz) parameters. As discussed within the context of Fig. 2, also these calculations show periodic frequency positions maximizing the $C_{1z}\rightarrow C_{2z}$ transfers over the ΔΩ range; these arise whenever the $\Delta\Omega = \pm j|g\nu_r - l/\Delta t|$ condition is satisfied (vertical stripes). In addition, MIRROR recoupling conditions[41] given by Eq. (5) –where $\nu_{eH}(t) = (\nu_{1H}^2 + \left[\mathrm{BW}/2 - \left(\mathrm{BW}/t_p\right)t\right]^2)^{0.5}$– can be seen in the form of departing diagonals. These MIRROR conditions are satisfied at or near the on-resonance position ($\Delta\Omega = 0$) when $\nu_{1H}$ is small (≤15 kHz), and fork into opposite ΔΩ directions as the RF field increases. Notice that for relatively weak $^1H$ RF fields these MIRROR conditions often "fill-up" poorly recoupled ΔΩ values arising between adjacent $\Delta\Omega = \pm j|g\nu_r - l/\Delta t|$ harmonic modes, thereby maximizing the robustness of the AL FRESCO mixing when $\nu_{1H}$ ≤20 kHz. Additional data presented in the Supporting

Information (Supporting Information, Fig. S2) show that weak RF fields, on the order of $\nu_{1H}$ = 15 kHz, will serve AL FRESCO well up to MAS rates $\nu_r \approx$ 100 kHz.

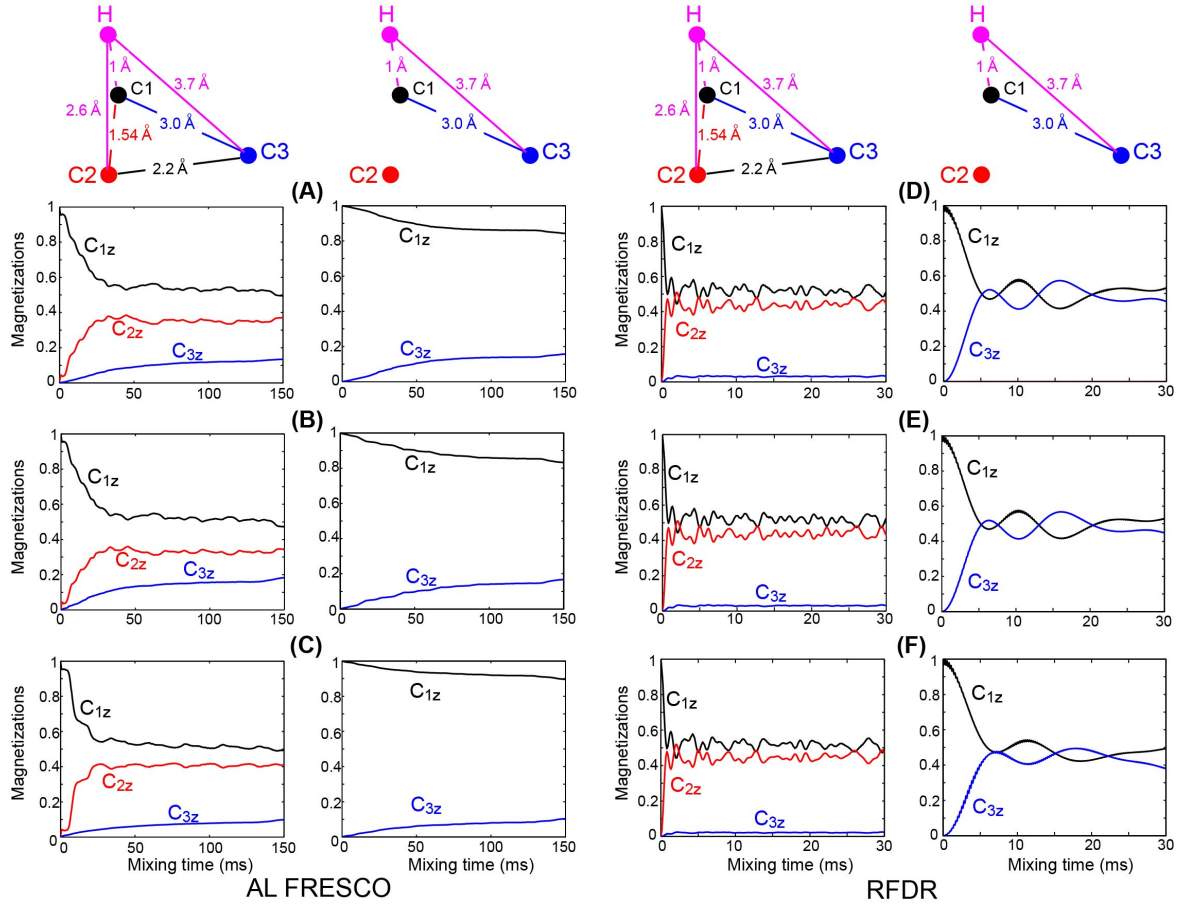


**Figure 5.** Comparing dipolar truncation effects for the AL FRESCO (A-C) vs RFDR (D-F) mixing schemes. The illustrated three- and four-spin systems (right- and left-hand columns within each scheme, respectively) were separately considered by these simulations, to better illustrate the effects of the stronger $C_1$-$C_2$ coupling on the polarization transfer undergone by the weaker $C_1$-$C_3$ one. The actual geometries and distance constraints assumed among nuclei are as on the (planar) cartoons drawn on the top; angles between adjacent dipolar vectors were as given by the distance constraints and geometry. Additional parameters: chemical shift anisotropy of $C_1$ and $C_2$: $\delta_{CSA}$= 40 ppm, $\eta_{CSA}$= 0.3; for $C_3$: $\delta_{CSA}$= 100 ppm, $\eta_{CSA}$= 0; for H: $\delta_{iso}$ = 2 ppm, $\delta_{CSA}$= 4 ppm, $\eta_{CSA}$= 0.2. For all cases $C_1$ was assumed on-resonance and the offset-frequencies of $C_2$ and $C_3$ placed at $\delta_{iso}^{C2}$ = -10 ppm, $\delta_{iso}^{C3}$ = 10 ppm for A and D; $\delta_{iso}^{C2}$ = -10 ppm, $\delta_{iso}^{C3}$ = 50 ppm for B and E; $\delta_{iso}^{C2}$ = -20 ppm, $\delta_{iso}^{C3}$ = 110 ppm for C and F. Relative orientations between shielding (zz) and dipolar tensors were assumed coincident for simplicity. A single chirp pulse ($\Delta t$ = 75 μs; BW = 80 kHz; $t_p$ = 150 ms; $\nu_{1H}$ = 13 kHz) was assumed for AL FRESCO, and a train of strong 180-degree pulses ($\nu_{1C}$= 200 kHz; $\tau_{mix}$ = 30 ms) was considered for RFDR (no proton decoupling). Larmor frequencies and the MAS rates were $\nu_0(^1H)$ = 600 MHz, $\nu_0(^{13}C)$ = 150 MHz, $\nu_r$ = 60 kHz. Initial magnetization was given only to $C_{1z}$ (black), and the signal build-up along either $C_{2z}$ (red) or $C_{3z}$ (blue) was sampled as the mixing time increases (notice the very different horizontal time scales).

**3.5 Dipolar truncation:** A final feature worth highlighting is that, in parallel with DARR and with other $^{1}$H-assisted recoupling methods, AL FRESCO is tolerant to so-called "dipolar truncation" effects; in other words, the presence of a dominant $^{13}C_1$-$^{13}C_2$ dipolar interaction will not mask the presence of cross-peaks arising from smaller (e.g., $^{13}C_1$-$^{13}C_3$) couplings. Figure 5 illustrates this by comparing the different outcomes that according to numerical simulations, the AL FRESCO and RFDR recoupling schemes will yield for a 3-spin $C_1$-$C_2$-$C_3$ system, when there is one strong dipolar interaction (r[$C_1$-$C_2$] = 1.54 Å) acting in competition with a weaker dipolar coupling (r[$C_1$-$C_3$] = 3.0 Å). The model also includes a putative (r[$C_2$-$C_3$] = 2.2 Å) intermediate distance, as well as a $^{1}$H spin that enables the AL FRESCO mechanism (but which plays no role in the RFDR scheme under the assumed MAS rate [52]). Notice the faster magnetization transfer from $C_1$ afforded by the RFDR method, which relies on the first-order recoupling of the $^{13}$C-$^{13}$C homonuclear dipolar interaction, vis-a-vis the slower AL FRESCO transfers which depend on a $^{1}$H-$^{13}$C-mediated $^{13}$C-$^{13}$C rotational resonance effect. On the other hand notice how the $C_1 \rightarrow C_3$ transfer efficiencies are significantly cut off by the presence of the stronger $C_1$-$C_2$ coupling in the RFDR scheme –a manifestation of the aforementioned dipolar truncation effect. By contrast, for all offset frequency differences considered, the $C_1 \rightarrow C_3$ transfer dynamics in AL FRESCO remains nearly unchanged, regardless of whether the stronger $C_1$-$C_2$ interaction is considered or not.

## 4. Experimental Results

Figure 6 illustrates AL FRESCO 2D $^{13}$C-$^{13}$C correlations obtained on a sample of uniformly $^{13}$C-labeled Barstar protein, upon using mixing times $\tau_{mix}$ = 320, 960 and 1600 ms and a MAS rate $\nu_r$ = 60 kHz. Also shown in the Figure for comparison is a 2D $^{13}$C-$^{13}$C correlation based on the CORD mixing scheme, measured with $\tau_{mix}$ = 320 ms –the longest mixing time that we ventured to apply on the probe. Indeed, whereas the average pulse power applied along the $^{1}$H channel throughout the CORD scheme was 2.2 W (=$[4.3\ \mathrm{W} \times 1 + 1.1\ \mathrm{W} \times 2]/3$ and associated to a $\nu_{1H}$ =60 kHz RF field applied over 107 ms and a 30 kHz field applied over 213 ms in the Bruker 1.3mm MAS probe used), the AL FRESCO power was only 0.2 W throughout the whole WURST [43] pulse train making up this mixing ($\nu_{1H}$ =13 kHz maximum RF). When factoring in the fact that the RF fields used on the $^{1}$H channel for cross-polarization and for ($XiX_{45}$ [49]) decoupling were 12 and 16 kHz, respectively, the ensuing experiment results in a very mild power

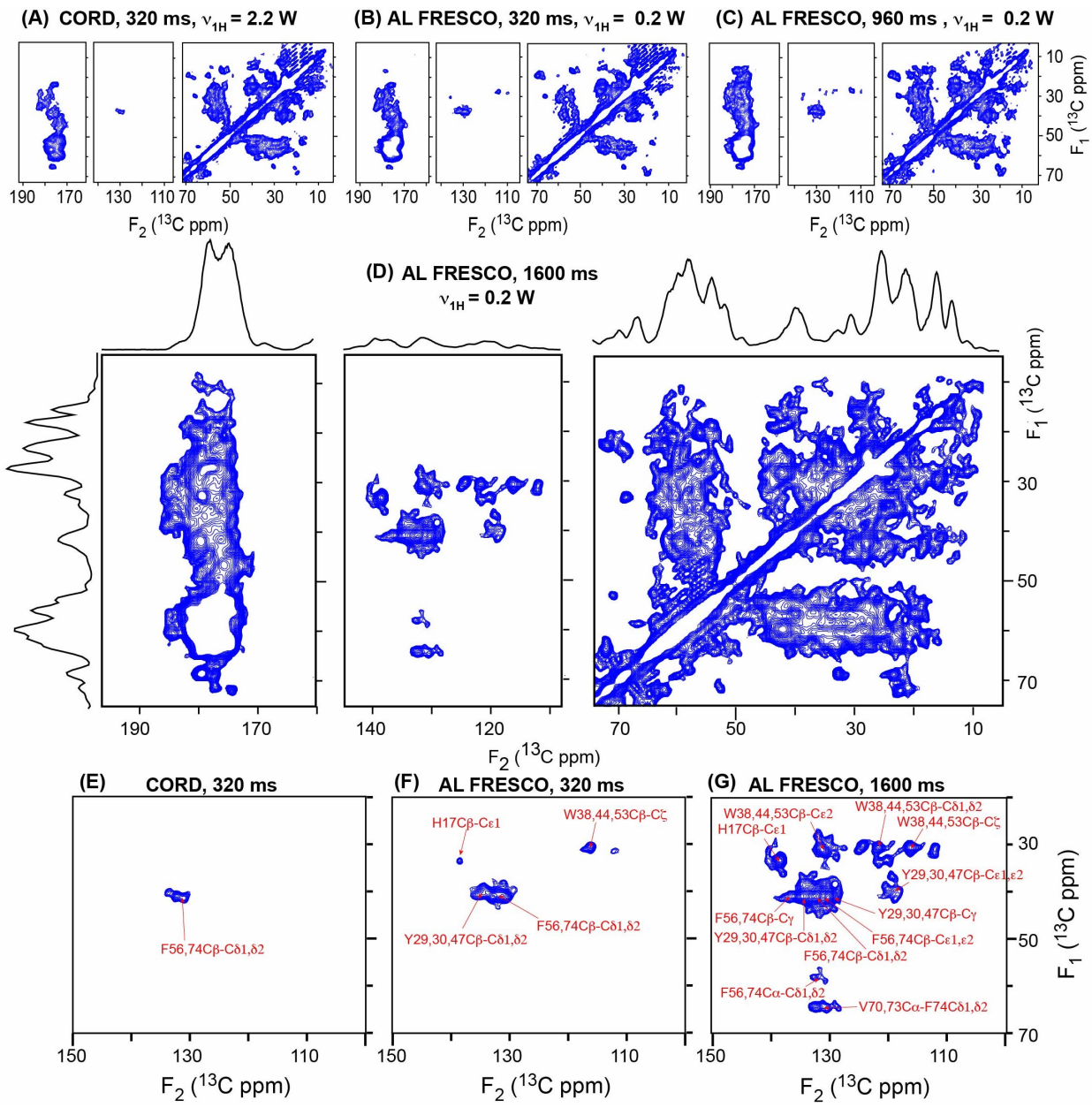


**Figure 6.** 2D $^{13}$C-$^{13}$C dipolar correlation spectra of U-$^{13}$C-labeled Barstar measured at $\nu_r$ = 60 kHz employing CORD [39,40] (A, E) and AL FRESCO (B, C, D, F, G) schemes with the indicated $\tau_{mix}$ values. In (B) and (C) an 80 ms long WURST-40 [44] pulse of 80 kHz bandwidth sampled at a dwell $\Delta t$ = 75 µs was repeated 4 or 12 times for (B) and (C) respectively, with forward and backward sweeps alternatively and XY phase alternation. For (D), a 100 ms WURST-40 pulse of 120 kHz bandwidth was sampled at $\Delta t$ = 75 µs and repeated 16 times with XY-16 phase alternation. The number of $t_1$-points was 240, incremented with a dwell time $\Delta t_1$ = 27 µs along the indirect domain for all cases. 80 scans were averaged for each $t_1$-point for (A, B), and 128 for (C, D), respectively. Partial cross-peak assignments are provided among sites, based on literature data [53]. (E), (F), and (G) compare the aliphatic-aromatic correlations of CORD and AL FRESCO schemes with assignments. The limited spectral resolution reflects the presence of residual homonuclear couplings and the lyophilized nature of the sample; see the Experimental for additional details.

deposition. Also remarkable is the efficiency with which correlations can be established for a given mixing time, as well as the multitude of cross-peaks that arise even between sites with large chemical shift differences and/or with no protons attached to them (e.g., Figs 6A-6C). This is illustrated as an expanded panel in Fig. 6D, which centers on correlations between aliphatic and aromatic sites. Notice as well that whereas for a $\tau_{mix}$ = 320 ms experiment CORD produces solely correlations from phenylalanines F56 and F74, an AL FRESCO experiment measured for the same mixing time produces additional correlations from H17, from tryptophanes W38, W44 and W53, and from tyrosines Y29, Y30 and Y47 (Figs. 6E,6G). These correlations as well as others emerging in the long-$\tau_{mix}$ regime, can be largely assigned on the basis of intramolecular contacts and of the solution-state NMR $^{13}$C shifts available for this protein [53].

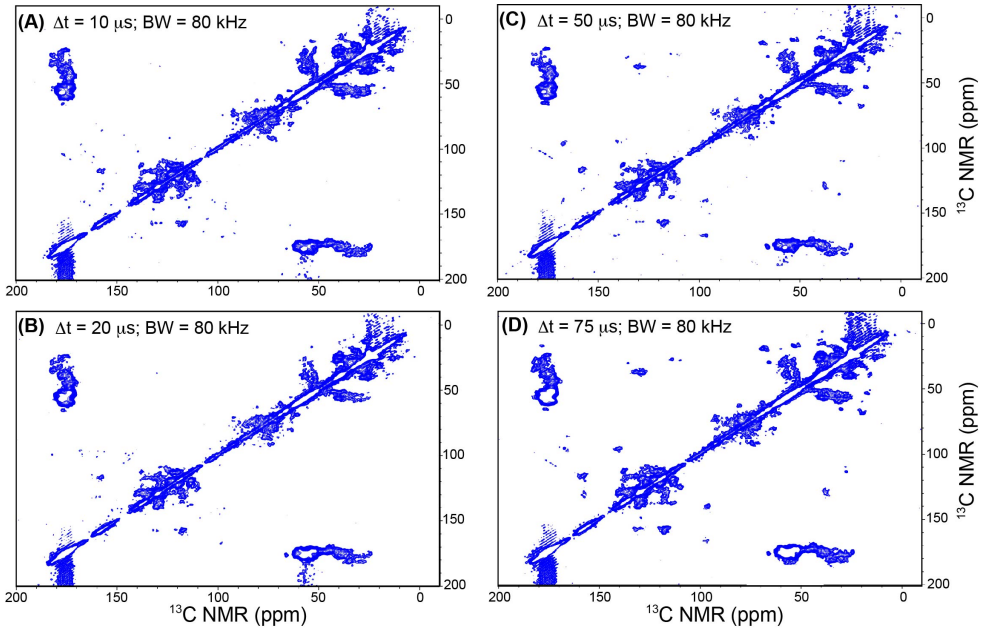


**Figure 7.** Experimental 2D $^{13}$C-$^{13}$C Barstar correlation spectra measured using the AL FRESCO scheme (Fig. 1) using the indicated $\Delta t$ and BW parameters; $n$=4 80 ms long chirped mixing pulses we utilized for the recoupling. MAS rates where $\nu_r$ = 60 kHz, overall mixing times were 320 ms, and additional acquisition parameters were as described in Figure 6. Notice that although only the spectrum in (A) fulfills the $1/\Delta t$>BW Nyquist criterion, cross-peaks become more intense with increasing $\Delta t$ values (the spectrum shown in (D) corresponds the one shown in Fig. 6B).

Figure 7 presents 2D AL FRESCO $^{13}$C-$^{13}$C correlation spectra measured on the same $^{13}$C-Barstar sample, upon varying $\Delta t$ while fixing the chirps' BW at 80 kHz (all other experimental parameters were also kept constant). Notice the improvement that, as evidenced by the appearance of new, more intense cross-peaks, arises upon increasing the sampling time $\Delta t$ until eventually going beyond the Nyquist sampling condition $\Delta t < 1/BW$. This is as theoretically

discussed in the previous section; best results are obtained when $\Delta t$ is in the 50~75 μs range; i.e., when undersampling ≈5 times the 1/BW Nyquist criterion.

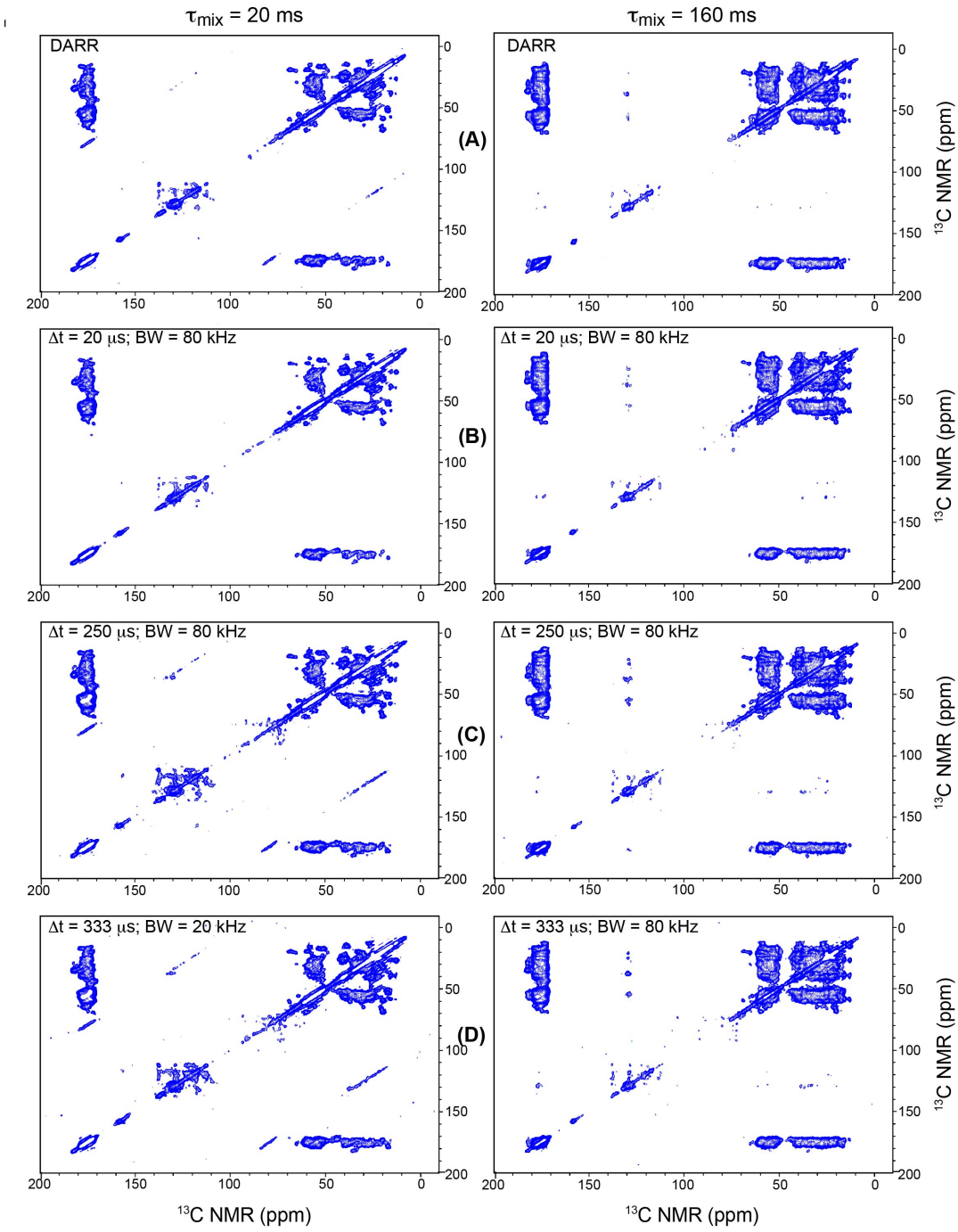


**Figure 8.** DARR (A) and AL FRESCO (B-D) Barstar spectra measured at $\nu_r$ = 12 kHz MAS for two different mixing times: $\tau_{mix}$ = 20 ms (left) and 160 ms (right). AL FRESCO spectra were measured using the indicated $\Delta t$ and BW values for the chirp pulse ($t_p$ = 40 ms; $n$ = 4).

The AL FRESCO scheme generates strong cross-peak intensities effectively over sites possessing a big chemical shift differences while employing weak RF field strengths, even at high-speed MAS rates. Experiments and simulations confirm that the method is also a superior

scheme for introducing dipolar recoupling on samples rotating at moderate MAS speeds. Figure 8 for instance compares the performance of DARR (A) and AL FRESCO (B-D), when carried out on a $^{13}$C-labeled Barstar sample undergoing MAS at $\nu_r$ = 12 kHz. Measurements are presented for two different mixing times, $\tau_{mix}$ = 20 ms and 160 ms, and AL FRESCO spectra are taken for 80 kHz BW sweeps and three different sampling cases: $\Delta t$ = 20 μs (B), $\Delta t$ = 250 μs (C) and $\Delta t$ = 333 μs (D). The latter two cases correspond to $\Delta t = 3/\nu_r$ and $\Delta t = 4/\nu_r$, respectively. Notice how, as in the fast-spinning experiments, the ensuing undersampled chirped pulse shapes achieve good recoupling –superior in fact, to the $\Delta t$ = 20 μs AL FRESCO sampling scheme. When compared to the $\nu_r$ = 60 kHz case, the cross-peaks within the aromatic sites as well as between the aromatic and aliphatic sites have become weaker, but the cross-peak intensities among aliphatic sites are stronger. (In fact for the $\tau_{mix}$ = 20 ms case, cross-peaks for either $\Delta t$ = 250 or 333 μs are stronger than when measured with $\tau_{mix}$ = 320 ms at $\nu_r$ = 60 kHz.) It follows that even at moderate MAS rates, the AL FRESCO polarization transfer is efficient.

## 5. Conclusions

Thanks to a combination of previously known mechanisms and of new recoupling phenomena, a novel method to improve the quality of 2D homonuclear solids NMR correlation spectra was proposed and demonstrated. The ensuing AL FRESCO approach led to efficient $^{13}$C-$^{13}$C transfers even under high MAS rates, aided by the lack of dipolar truncation, by a use of low RF field strengths that make it compatible with long mixing times leading to stronger cross-peaks, and by a reliance on frequency-swept pulses that endow it with broadbandness with respect to both the active ($^{13}$C) and passive ($^{1}$H) nuclides involved. A particularly useful new parameter for tuning this kind of experiments was found in the dwell time used to clock out the frequency-swept pulse, lending additional robustness for the experiment. Further, although most results were recorded for $\nu_r$ = 60 kHz MAS rates, experiments and simulations also show that the AL FRESCO mixing is equal or better than alternative schemes for samples rotating at different MAS rates. Figure 8 demonstrated this for moderately low MAS rates (12 kHz); simulations (Supporting Fig. S2) evidence that AL FRESCO mixing should also be highly efficient at spinning rates $\nu_r \geq$ 100 kHz. Many other exciting options are opened by the broad-bandness of the approach: for instance, the method looks like a promising $^{1}$H-$^{1}$H mixing scheme for samples subject to ultrafast MAS, in

experiments where the $^{1}$Hs are detected while either $^{13}$C or $^{15}$N serve as the acted-upon nuclei mediating the recoupling. This is thanks to AL FRESCO's swept pulses, that when applied along either $^{13}$C or $^{15}$N channels can efficiently cover a wide range of offset frequencies –even for high-field chemical shift dispersions. These and other similar experiments of this kind, will be described in an upcoming study.

**Acknowledgments.** We are grateful to Dr. Shira Albeck (ISPC, Weizmann Institute of Science) for the Barstar protein preparation; we also thank Dr. Robert Tycko for valuable discussions, as well as anonymous reviewer #2 for his/her extensive, constructive suggestions and comments. This work was supported in part by the Israel Science Foundation (Grant 965/18), and by the Perlman Family Foundation. This work was supported by the US National Science Foundation through grants DMR-1644779 and DMR-1157490 (to the US National High Magnetic Field Laboratory) and by the State of Florida.

## References:


[1] B. Sarkar, V. S. Mithu, B. Chandra, A. Mandal, M. Chandrakesan, D. Bhowmik, P. K. Madhu, S. Maiti, *Angew. Chem.* **2014**, *53*, 1.

[2] D. T. Murray, M. Kato, Y. Lin, K. R. Thurber, I. Hung, S. L. McKnight, R. Tycko, *Cell* **2017**, *171*, 615.

[3] B. Bersch, J. M. Dörr, A. Hessel, J. A. Killian, P. Schanda, *Angew Chem., Int. Ed. Engl.* **2017**, *56*, 2508.

[4] D. Stöppler, A. Macpherson, S. Smith-Penzel, N. Basse, F. Lecomte, H. Deboves, R. D. Taylor, T. Norman, J. Porter, L. C. Waters, M. Westwood, B. Cossins, K. Cain, J. White, R. G. Griffin, C. Prosser, S. Kelm, A. H. Sullivan, D. R. Fox, M. D. Carr, A. Henry, R. Taylor, B. H. Meier, H. Oschkinat, A. D. Lawson, *PLoS. Biol.* **2018**, *16*, e2006192.

[5] M. Mompeán, W. Li, J. Li, S. Laage, A. B. Siemer, G. Bozkurt, H. Wu, A. E. McDermott, *Cell* **2018**, *173*, 1244.

[6] W. Close, M. Neumann, A. Schmidt, M. Hora, K. Annamalai, M. Schmidt, B. Reif, V. Schmidt, N. Grigorieff, M Faendrich, *Nat. Commun.* **2018**, *9*, 699.

[7] E. Barbet-Massin, E. van der Sluis, J. Musial, R. Beckmann, B. Reif, *Methods Mol. Biol.* **2018**, *1764*, 87.

[8] O. Morag, N. Sgourakis, G. Abramov, A. Goldbourt, In *Protein NMR: Methods and Protocols,* R. Ghose, Ed. **2018**, Vol. 1699, p 67.

[9] D. P. Raleigh, M. H. Levitt, R. Griffin, *Chem. Phys. Lett.* **1988**, *146*, 71.

[10] N. M. Szeverenyi, M. J. Sullivan, G. E. Maciel, *J. Magn. Reson.* **1982**, *47*, 462.

[11] A. Grommek, B. H. Meier, M. Ernst, *Chem. Phys. Lett.* **2006**, *427*, 404.

[12] B. H. Meier, *Polarization transfer and spin diffusion in solid state NMR*, Academic Press: New York, 1994, Vol. 18.

[13] T. Gullion, J. Schaefer, *J. Magn. Reson.* **1989**, *81*, 196.

[14] F. G. Oas, R. G. Griffin, M. H. Levitt, *J. Chem. Phys.* **1988**, *89*, 692.

[15] M. H. Levitt, In *Encyclopedia of Nuclear Magnetic Resonance*, D. M. Grant, R. K. Harris, Eds., Wiley: Chichester, U.K., 2002, Vol. 9, p 165.

[16] A. Brinkmann, M. H. Levitt, *J. Chem. Phys.* **2001**, *115*, 357.

[17] A. E. Bennett, J. H. Ok, R. G. Griffin, S. Vega, *J. Chem. Phys.* **1992**, *96*, 8624.

[18] N. C. Nielsen, H. Bildsoe, H. J. Jakobsen, M. H. Levitt, *J. Chem. Phys.* **1994**, *101*, 1805.

[19] R. Verel, M. Ernst, B. H. Meier, *J. Magn. Reson.* **2001**, *150*, 81.

[20] M. J. Bayro, M. Huber, R. Ramachandran, T. C. Davenport, B. H. Meier, M. Ernst, R. G. Griffin, *J. Chem. Phys.* **2009**, *130*, 114506.

[21] R. Tycko, *J. Phys. Chem. B* **2008**, *112*, 6114.

[22] K. Takegoshi, S. Nakamura, T. Terao, *Chem. Phys. Lett.* **2001**, *344*, 631.

[23] K. Takegoshi, S. Nakamura, T. Terao, *J. Chem. Phys.* **2003**, *118*, 2325.

[24] C. R. Morcombe, V. Gaponenko, R. A. Byrd, K. W. Zilm, *J. Am. Chem. Soc.* **2004**, *126*, 7196.

[25] G. De Paëpe, J. R. Lewandowski, A. Loquet, A. Böckman, Griffin, R. G. *J. Chem. Phys.* **2008**, *129*, 245101.

[26] J. R. Lewandowski, G. De Paëpe, M. T. Eddy, J. Struppe, J. W. Maas, R. G. Griffin, *J. Phys. Chem. B* **2009**, *113*, 9062.

[27] F. Castellani, B. van Rossum, A. Diehl, M. Schubert, K. Rehbein, H. Oschkinat, *Nature* **2002**, *420*, 98.

[28] L. Huang, A. E. McDermott, *Biochim. Biophys. Acta, Bioenerg.* **2008**, *1777*, 1098.

[29] M. D. Tuttle, G. Comellas, A. J. Nieuwkoop, D. J. Covell, D. A. Berthold, K. D. Kloepper, J. M. Courtney, J. K. Kim, A. M. Barclay, A.; Kendall, W. Wan, G. Stubbs, C. D. Schwieters, V. M. Y. Lee, J. M. George, C. M. Rienstra, *Nat. Struct. Mol. Biol.* **2016**, *23*, 409.
[30] J.-X. Lu, W.-M. Yau, R. Tycko, *Biophys. J.* **2011**, *100*, 711.
[31] S. Y. Liao, K. J. Fritzsching, M. Hong, *Protein Sci.* **2013**, *22*, 1623—1638.
[32] Y. Miao, H. Qin, R. Fu, M. Sharma, T. V. Can, I. Hung, S. Luca, P. L. Gor'kov, W. W. Brey, T. A. Cross, *Angew Chem., Int. Ed. Engl.* **2012**, *51*, 8383.
[33] M. Weingarth, G. Bodenhausen, P. Tekely, *Chem. Phys. Lett.* **2010**, *488*, 10.
[34] M. Weingarth, D. E. Demco, G. Bodenhausen, P. Tekely, *Chem. Phys. Lett.* **2009**, *469*, 342.
[35] B. Hu, O. Lafon, J. Trébosc, Q. Chen, J.-P. Amoureux, *J. Magn. Reson.* **2011**, *212*, 320.
[36] B. Hu, J. Trébosc, O. Lafon, Q. Chen, Y. Masuda, K. Takegoshi, J.-P. Amoureux, *ChemPhysChem* **2012**, *13*, 3585.
[37] M. Shen, Q. Liu, J. Trébosc, O. Lafon, Y. Masuda, K. Takegoshi, J.-P. Amoureux, B. Hu, Q. Chen, *Solid State Nucl. Magn. Reson.* **2013**, *55-56*, 42.
[38] X. J. Yan, B. Hu, *Chinese J. Magn. Reson.* **2016**, *33*, 361.
[39] G. Hou, S. Sun, Y. Han, I.-J. Byeon, J. Ahn, J. Concel, A. Samoson, A. M. Gronenborn, T. Polenova, *J. Am. Chem. Soc.* **2011**, *133*, 3943.
[40] G. Hou, S. Yan, J. Trébosc, J.-P. Amoureux, T. Polenova, *J. Magn. Reson.* **2013**, *232*, 18.
[41] I. Scholz, M. Huber, T. Manolikas, B. H. Meier, M. Ernst, *Chem. Phys. Lett.* **2008**, *460*, 278.
[42] G. Schreiber, A. R. Fersht, *Biochemistry* **1993**, *32*, 11195.
[43] E. Kupce, R. Freeman, *J. Magn. Reson. A* **1995**, *115*, 273.
[44] M. Garwood, L. delaBarre, *J. Magn. Reson.* **2001**, *153*, 155.
[45] T. Gullion, D. B.; Baker, M. S. Conradi, *J. Magn. Reson.* **1990**, *89*, 479.
[46] O. B. Peersen, X. L. Wu, I. Kustanovich, S. O. Smith, *J. Magn. Reson. A* **1993**, *104*, 334.
[47] G. Metz, X. L. Wu, S. O. Smith, *J. Magn. Reson. A* **1994**, *110*, 219.
[48] A.; Detken, E. H. Hardy, M. Ernst, B. H. Meier, *Chem. Phys. Lett.* **2002**, *356*, 298.
[49] M. Ernst, A. Samoson, B. H. Meier, *J. Magn. Reson.* **2003**, *163*, 332.
[50] B. M. Fung, A. K. Khitrin, K. Ermolaev, *J. Magn. Reson.* **2000**, *142*, 97.
[51] V. B. Cheng, H. Henry, J. Suzukawa, M. Wolfsberg, *J. Chem. Phys.* **1973**, *59*, 3992.
[52] M. Shen, B. Hu,O. Lafon, J. Trébosc, Q. Chen, J.-P. Amoureux, *J. Magn. Reson.* **2012**, *223*, 107.
[53] M. J. Lubienski, M. Bycroft, S. M. V. Freund, A. R. Fersht, *Biochemistry* **1994**, *33*, 8866.

## Graphical Abstract

This study presents a methodology based on frequency-swept pulses, for imparting 2D homonuclear solid NMR correlations using unusually weak pulses. The potential of the ensuing 2D AL FRESCO experiment is demonstrated with ultrafast $^{13}C$ MAS NMR results on the protein barstar, established by $^{1}H$ irradiations lasting over 1sec mixing times.

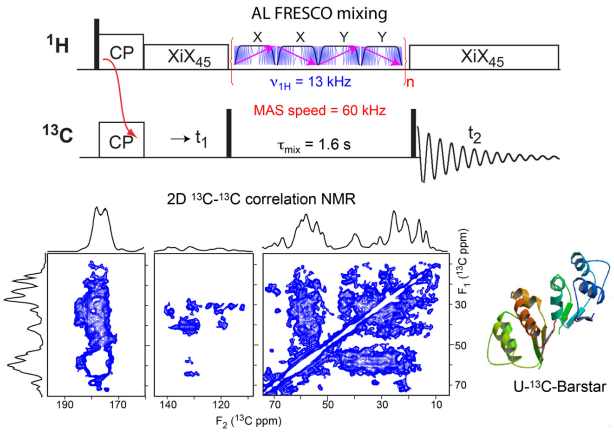


**An efficient, robust new scheme for establishing broadband homonuclear correlations in biomolecular solid state NMR**

S. Wi and L. Frydman

**Figure Captions:**

**Figure 1.** AL FRESCO mixing scheme incorporated within the standard platform of 2D $^{13}C$ homonuclear correlation spectroscopy. AL FRESCO employs a phase-modulated linear frequency chirped pulse or a train of chirped pulses applied on the $^{1}Hs$, with optimal RF pulse strengths of ≈10~20 kHz regardless of the MAS rate used. When using a train of chirped pulses, the mixing scheme benefits from concatenating forward- and backward-sweeps while employing an XY-$n$ phase-alternation scheme [45] to compensate potential RF inhomogeneities.

**Figure 2.** Development of the $C_{1z}\rightarrow C_{2z}$ polarization transfer dynamics arising from an initial state $C_{1z}=1$, $C_{2z}=0$, when monitoring $C_{2z}$ as a function of mixing time $0\leq\tau_{mix}\leq t_p=40$ms, for a range of offset frequencies -500ppm$\leq\Omega_{C2}\leq$500ppm while assuming $\Omega_{C1}= 0$. The plots were calculated as a function of the chirp pulse bandwidth (BW) and its sampling dwell ($\Delta t$), for an AL FRESCO mixing scheme like the one in Figure 1. Additional assumptions involved a four-spin system $H_1$-$C_1$-$C_2$-$H_2$ (top, numbers indicating distances in Å) undergoing MAS at $\nu_r$= 60 kHz. Additional parameters included $\delta_{CSA}^{C1} = \delta_{CSA}^{C2} =$ 40 ppm, $\eta_{C1} = \eta_{c2} =$ 0.3, $\delta_{ISO}^{H1} =$ -2 ppm, $\delta_{CSA}^{H1} =$ 3 ppm, $\eta_{H1} = 0$, $\delta_{ISO}^{H2} =$ 4 ppm, $\delta_{CSA}^{H2} =$ 2 ppm, $\eta_{H2} =$ 0.2, $\nu_0[^1H]$ = 600 MHz; $\nu_0[^{13}C]$ = 150 MHz, $\nu_{1H}$= 15 kHz. Exact distances were $r[C_1\text{-}C_2]$ = 1.54 Å, $r[C_1\text{-}H_1]$ = 1.00 Å, $r[C_2\text{-}H_1]$ = 2.22 Å, $r[C_1\text{-}H_2]$ = 2.22 Å, $r[C_2\text{-}H_2]$ = 1.00 Å, $r[H_1\text{-}H_2]$ = 2.54 Å. Notice the strong harmonic recoupling modes formed in the offset-frequency profile, as well as their Δt-dependence.

.

**Figure 3.** The influence of BW and $\Delta t$ on AL FRESCO's $C_1\rightarrow C_2$ polarization transfer dynamics calculated on a $H_1$-$C_1$-$C_2$-$H_2$ spin system (Fig. 2) under $\nu_r$ = 60 kHz. For both cases the $C_{2z}$ buildup is calculated as a function of mixing time $\tau_{mix}$, $0 \leq \tau_{mix} \leq t_p$=40 ms ($C_{1z}$ = 1 and $C_{2z}$ = 0 at $\tau_{mix}$ = 0) at three different offset frequencies ($\Delta\Omega/2\pi$ = 0, 30, and 120 ppm; $\nu_0(^{13}C)$ = 150 MHz). Notice that sampling the pulse at a rate that satisfies the Nyquist criterion for all BWs yields a in general a slower $C_{1z}\rightarrow C_{2z}$ polarization transfer efficiency than upon breaking this criterion –which in turn results in multiple foldovers within the frequency window 1/Δt.

**Figure 4.** RF field ($\nu_{1H}$) dependence for AL FRESCO recoupling (y-axis) as a function of the $\Delta\Omega = \nu_{iso}^{C1} - \nu_{iso}^{C2}$ separation between the $^{13}$C (x-axis). The plots calculate the $C_{1z} \rightarrow C_{2z}$ transfer efficiency for a $H_1$-$C_1$-$C_2$-$H_2$ spin system (as in Fig. 2; colormap indicates $<C_{2z}>$), assuming a single chirp recoupling with BW = 80 kHz, $t_p$ = 40 ms, and two different sampling conditions: $\Delta t$ = 66.67 μs ($4/\nu_r$, A), and $\Delta t$ = 75 μs ($4.5/\nu_r$, B).

**Figure 5.** Comparing dipolar truncation effects for the AL FRESCO (A-C) vs RFDR (D-F) mixing schemes. The illustrated three- and four-spin systems (right- and left-hand columns within each scheme, respectively) were separately considered by these simulations, to better illustrate the effects of the stronger $C_1$-$C_2$ coupling on the polarization transfer undergone by the weaker $C_1$-$C_3$ one. The actual geometries and distance constraints assumed among nuclei are as on the (planar) cartoons drawn on the top; angles between adjacent dipolar vectors were as given by the distance constraints and geometry. Additional parameters: chemical shift anisotropy of $C_1$ and $C_2$: $\delta_{CSA}$= 40 ppm, $\eta_{CSA}$= 0.3; for $C_3$: $\delta_{CSA}$= 100 ppm, $\eta_{CSA}$= 0; for H: $\delta_{iso}$ = 2 ppm, $\delta_{CSA}$= 4 ppm, $\eta_{CSA}$= 0.2. For all cases $C_1$ was assumed on-resonance and the offset-frequencies of $C_2$ and $C_3$ placed at $\delta_{iso}^{C2}$ = -10 ppm, $\delta_{iso}^{C3}$ = 10 ppm for A and D; $\delta_{iso}^{C2}$ = -10 ppm, $\delta_{iso}^{C3}$ = 50 ppm for B and E; $\delta_{iso}^{C2}$ = -20 ppm, $\delta_{iso}^{C3}$ = 110 ppm for C and F. Relative orientations between shielding (zz) and dipolar tensors were assumed coincident for simplicity. A single chirp pulse ($\Delta t$ = 75 μs; BW = 80 kHz; $t_p$ = 150 ms; $\nu_{1H}$ = 13 kHz) was assumed for AL FRESCO, and a train of strong 180-degree pulses ($\nu_{1C}$= 200 kHz; $\tau_{mix}$ = 30 ms) was considered for RFDR (no proton decoupling). Larmor frequencies and the MAS rates were $\nu_0(^1H)$ = 600 MHz, $\nu_0(^{13}C)$ = 150 MHz, $\nu_r$ = 60 kHz. Initial magnetization was given only to $C_{1z}$ (black), and the signal build-up along either $C_{2z}$ (red) or $C_{3z}$ (blue) was sampled as the mixing time increases (notice the very different horizontal time scales).

**Figure 6.** 2D $^{13}$C-$^{13}$C dipolar correlation spectra of U-$^{13}$C-labeled Barstar measured at $\nu_r$ = 60 kHz employing CORD [39,40] (A, E) and AL FRESCO (B, C, D, F, G) schemes with the indicated $\tau_{mix}$ values. In (B) and (C) an 80 ms long WURST-40 [44] pulse of 80 kHz bandwidth sampled at a dwell $\Delta t$ = 75 μs was repeated 4 or 12 times for (B) and (C) respectively, with forward and backward sweeps alternatively and XY phase alternation. For (D), a 100 ms WURST-40 pulse of 120 kHz bandwidth was sampled at $\Delta t$ = 75 μs and repeated 16 times with XY-16 phase alternation.

The number of $t_1$-points was 240, incremented with a dwell time $\Delta t_1$ = 27 μs along the indirect domain for all cases. 80 scans were averaged for each $t_1$-point for (A, B), and 128 for (C, D), respectively. Partial cross-peak assignments are provided among sites, based on literature data [53]. (E), (F), and (G) compare the aliphatic-aromatic correlations of CORD and AL FRESCO schemes with assignments. The limited spectral resolution reflects the presence of residual homonuclear couplings and the lyophilized nature of the sample; see the Experimental for additional details.

**Figure 7.** Experimental 2D $^{13}C$-$^{13}C$ Barstar correlation spectra measured using the AL FRESCO scheme (Fig. 1) using the indicated $\Delta t$ and BW parameters; $n$=4 80 ms long chirped mixing pulses we utilized for the recoupling. MAS rates where $\nu_r$ = 60 kHz, overall mixing times were 320 ms, and additional acquisition parameters were as described in Figure 6. Notice that although only the spectrum in (A) fulfills the $1/\Delta t$>BW Nyquist criterion, cross-peaks become more intense with increasing $\Delta t$ values (the spectrum shown in (D) corresponds the one shown in Fig. 6B).

**Figure 8.** DARR (A) and AL FRESCO (B-D) Barstar spectra measured at $\nu_r$ = 12 kHz MAS for two different mixing times: $\tau_{mix}$ = 20 ms (left) and 160 ms (right). AL FRESCO spectra were measured using the indicated $\Delta t$ and BW values for the chirp pulse ($t_p$ = 40 ms; $n$ = 4).